Journal of the European Ceramic Society **14** (1994) 163–175

Liquid Phase Sintering, Electrical Conductivity, and Chemical Stability of Lanthanum Chromite Doped with Calcium and Nickel

G. M. Christie,* P. H. Middleton & B. C. H. Steele

Department of Materials, Imperial College of Science, Technology and Medicine, London SW7 2BP, UK

(Received 28 October 1993; accepted 19 November 1993)

Abstract

The substitution of 10 mol% nickel for chromium in calcium doped lanthanum chromite has been shown to promote rapid densification of the compound at low temperatures in air by the formation of a transient liquid phase. Liquids were generated via the decomposition of $CaCrO_4$ second phase material present in calcined powders. During electrical conductivity measurements at 1000°C, severe microstructural degradation occurred in atmospheres of H_2 and CO_2. The processes leading to chemical degradation are attributed to the precipitation of Ni from the $(La,Ca)(Cr,Ni)O_3$ solid solution and to the decomposition of small amounts of residual $CaCrO_4$ which remains at grain boundaries and triple points after sintering. DTA studies on $CaCrO_4$ in CO_2 and H_2 atmospheres suggested that the degradation due to $CaCrO_4$ decomposition was primarily a result of the reaction of CaO with CO_2 to form $CaCO_3$. The presence of H_2 gas is thought to catalyse this reaction via the formation of large amount of CaO during the decomposition of $CaCrO_4$. Degradation is more severe in atmospheres containing a mixture of CO_2 and H_2 gases than in either gas on its own.

Die Substitution von 10 mol% Nickel für Chrom in einem Kalzium-dotierten Lanthanchromit ergab durch die Bildung einer flüssigen Übergangsphase eine rasche Verdichtung des Preßkörpers bei niedrigen Temperaturen an Luft. Die flüssige Phase entstand durch den Zerfall der sekundären $CaCrO_4$ Phase im kalzinierten Pulver. Während der Messung der elektrischen Leitfähigkeit bei 1000°C zeigte sich in einer H_2 und CO_2 Atmosphäre eine deutliche Degradierung des Gefüges. Der Prozeß, der zur chemischen Degradierung führt, ist auf die Ausscheidung von Ni aus dem $(La, Ca)(Cr,Ni)O_3$ Mischkristall und dem Zerfall kleiner Mengen restlichen $CaCrO_4$ an den Korngrenzen und an den Tripelpunkten nach dem Sintern zurückzuführen. DTA Untersuchungen an $CaCrO_4$, in einer CO_2 und H_2 Atmosphäre, legen nahe, daß die Degradierung aufgrund des Zerfalls von $CaCrO_4$ hauptsächlich aus der Reaktion von CaO mit CO_2 zu $CaCO_3$ resultiert. Die Anwesenheit von H_2-Gas dient dabei wahrscheinlich als Katalysator durch die Bildung großer Mengen CaO während des Zerfalls von $CaCrO_4$. Die Degradierung in einer Atmosphäre, bestehend aus einem Gemisch von CO_2 und H_2, ist weit stärker als in einer Atmosphäre bestehend aus nur einem Gas.

Nous montrons qu'en substituant 10% mol de nickel au chrome dans du chromite de lanthane dopé au calcium, la densification du composé sous air et à basses températures est accélérée grâce à la formation d'une phase liquide transitoire. Ces composés liquides proviennent de la décomposition de $CaCrO_4$ présent dans les poudres calcinées. A 1000°C, durant des expériences de conductivité, nous avons observé une dégradation sévère de la microstructure, sous H_2 et CO_2. Cette dégradation chimique est attribuée à la précipitation de Ni de la solution solide $(La,Ca)(Cr,Ni)O_3$, et à la décomposition de petites quantités de $CaCrO_4$ résiduel demeuré aux joints de grains et aux points triples après le frittage. L'étude par ATD de $CaCrO_4$ dans CO_2 et H_2 suggère que la dégradation due à la décomposition de $CaCrO_4$ est le résultat, au départ, de la réaction: $CaO + CO_2 \rightarrow CaCO_3$. Nous pensons que la présence de H_2 catalyse cette réaction en formant CaO en grande quantité durant la décomposition de $CaCrO_4$. La dégradation est plus sévère dans un mélange de CO_2 et H_2 que dans l'un quelconque de ces gaz purs.

* Permanent address: The Netherlands Energy Research Foundation, P.O. Box 1, 1755 ZG, Petten, The Netherlands.

Journal of the European Ceramic Society 0955-2219/94/$7.00

1 Introduction

Solid oxide fuel cells (SOFC) are emerging as the most important type of fuel cell for the generation of electricity for the consumer market. The relatively simple mode of operation involving only solid components, gaseous fuel and air offer distinct advantages over more conventional cells requiring management of liquid electrolytes. The high temperature of operation (900–1000°C) has presented some serious hurdles in the course of development, but recent advances in ceramic processing and technology has enabled some of the more intractable problems to be solved. Thus, the Westinghouse Electric Corporation in conjunction with the US Department of Energy now offer a 25 kW unit with larger 100 KW units planned for field testing in 1994.[1] Of the various design concepts available, Westinghouse have produced stacks built up from tubular single cells in series and parallel bundles, each cell requiring interconnection to its neighbour. This is achieved by coating part of each tube with a layer of electronically conducting doped lanthanum chromite using the electrochemical vapour deposition process (EVD). The exposed portion is then used to make contact with the adjacent tubes via nickel felt pads.

The European SOFC programme favours a planar concept incorporating interconnection in the form of bipolar plates separating the individual cells in the stack.[2] The designs offer a choice between metallic or lanthanum chromite bipolar plates and both approaches are receiving considerable attention. In the case of lanthanum chromite, the processing route should produce a product that is close to theoretical density, i.e. fully sintered, and that will also withstand the aggressive environment encountered in the operating cell, particularly tolerance to changes in oxygen partial pressure, tolerance to high current densities, low volatility of the constituents, inertness to surrounding material, long term stability and retention of mechanical strength and fracture toughness. Thermal expansion compatibility with the other cell components is also a key issue and the fabrication route should preferably involve sintering in air at moderate temperatures. The functional requirements demand high electronic conductivity for current distribution, and negligible permeation of gas, since the plate also serves to channel the fuel or air to the active parts of the cell. In this context the ionic conductivity of the material should be minimal.

In order to achieve the desired level of conduction, doping on the A site of the perovskite is required thus compositions containing the alkali earths Sr, Mg, and Ca are normally used. The conduction mechanism involves an activated hole hopping mechanism. The conductivity of the Ca and Sr doped $LaCrO_3$ are higher than that of the Mg doped variant,[3–5] though the Westinghouse EVD process precludes the use of Ca and Sr due to the low vapour pressure of their precursor chlorides, thus restricting the choice in this case to Mg doped material.[6] The more conventional ceramic processing routes do not have this limitation.

Normal A site doped $LaCrO_3$ will not sinter to high density in air because of problems related to the high vapour pressure of chromium,[7] so in order to achieve acceptable densities, samples are often heated to temperatures in excess of 1700°C under reducing conditions with the $pO_2 < 10^{-12}$ atm.[8] However, in the work reported here, we have been concerned with the development of low temperature air sinterable systems that satisfy the aforementioned material requirements for cell interconnects.

There are many references in the literature which cite the use of additives to improve the sintering characteristics. Fluoride mixtures,[9,10] addition of $SrCO_3$ or CaO stabilised ZrO_2 to $(La,Sr)CrO_3$,[11,12] Cu, Zn and Al substitutions,[13,14] and TiO_2 additions[15] have all been shown to enhance the sinterability of doped $LaCrO_3$.

More recently work has focused on the densification of Ca doped $LaCrO_3$ by liquid phase sintering mechanisms. Cobalt substitutions for chromium have been shown to dramatically improve the sintered density at low temperatures.[16,17] Sakai *et al.* reported that a 2% chromium deficiency in calcium doped compounds facilitates densification of the compound at temperatures as low as 1300°C in air.[18,19] Cr deficiencies in Mg or Sr doped $LaCrO_3$ are accompanied by the precipitation of hygroscopic La_2O_3, similarly in Cr deficient Ca doped $LaCrO_3$ the Ca content must be > 0·15 mol% to avoid the precipitation of La_2O_3.

The stability of liquid phase sintered calcium doped lanthanum chromite has recently become questionable. Sakai and co-authors have reported on the chemical stability of a number of compositions in a simulated SOFC environment.[20,21] The authors report that the calcium doped compounds and to a lesser extent strontium doped compounds, densified via cobalt substitutions were not stable under simulated SOFC operating conditions. The work concluded that the microstructural degradation was a result of migration of second phase material that facilitated densification of the compounds.

The work presented here reports on the sinterability and chemical stability of calcium and nickel doped compounds, includes electrical conductivity data and microstructural studies and offers an explanation for the instability of these compounds.

2 Experimental

2.1 Sintering studies

Powders of nominal composition $La_{0.8}Ca_{0.2}Cr_{0.9}Ni_{0.1}O_3$, $La_{0.7}Ca_{0.3}Cr_{0.9}Ni_{0.1}O_3$ and $La_{0.6}Ca_{0.4}Cr_{0.9}Ni_{0.1}O_3$ were prepared by the citrate route[22] and analysed by XRD for phase purity. Pellets were pressed at 300 MPa in a 13 mm diameter die for dilatometry and quench tests. All powder compacts were sintered at a furnace temperature of 1500°C for 5 h. After sintering, pellets of each composition were polished and re-analysed by XRD, to check phase purity and in order to determine lattice parameters for calculation of theoretical densities. High temperature dilatometry (Netzsth 402E 1600) was used to collect linear shrinkage versus temperature data during the sintering of green powder compacts.

The mechanism by which the nickel substitutions lead to enhanced sinterability was investigated by quench studies combined with XRD, SEM/EDAX and DTA analysis. In the quench studies, samples were removed from the furnace during the sintering regime and allowed to cool in air to room temperature. The furnace temperatures from which samples were quenched were 1170°C and 1385°C, but sample temperatures are likely to have been around 30–50°C lower. The compositions chosen for the quench study were those containing a higher level of calcium doping, i.e samples of nominal composition $La_{0.7}Ca_{0.3}Cr_{0.9}Ni_{0.1}O_3$ and $La_{0.6}Ca_{0.4}Cr_{0.9}Ni_{0.1}O_3$. Fractured cross-sections and surfaces of the pellets were then examined by SEM and EDAX. DTA analysis was performed on powders of nominal composition $La_{0.8}Ca_{0.2}Cr_{0.9}Ni_{0.1}O_3$ and $La_{0.7}Ca_{0.3}Cr_{0.9}Ni_{0.1}O_3$. Powders were heated at 10°C/min in platinum crucibles over the temperature range 900–1500°C. Pure Al_2O_3 was used as the reference material.

A sample of composition $La_{0.7}Ca_{0.3}Cr_{0.9}Ni_{0.1}O_3$ was examined by transmission electron microscopy (TEM) in order to establish whether or not second phase material remained at grain boundaries after sintering.

2.2 Chemical stability in hydrogen

A sample of sintered ceramic of composition $La_{0.8}Ca_{0.2}Cr_{0.9}Ni_{0.1}O_3$ was annealed at 900°C in forming gas (10% hydrogen in 90% nitrogen) for 200 h. The forming gas was bubbled through water at a flow rate of 25 ml/min and the pO_2 inside the sample enclosure, as measured by a zirconia oxygen probe, was 5×10^{-16} atm. The reduced sample was analysed by XRD, fracture surfaces and polished and thermally etched surfaces of the reduced ceramic were examined by SEM.

2.3 Electrical conductivity

Electrical conductivity measurements were made on 5 cm long bar samples by an established DC four probe technique using platinum contact wires and a constant current of 10 mA. The electrical conductivity measurements were made over a wide range in pO_2 at a fixed temperature of 1000°C. The range of oxygen partial pressures covered was from 0·2 to 10^{-19} atm. which was achieved by mixing CO_2 and forming gas (90% N_2, 10% H_2). The change in conductivity was monitored continuously with time and held at the selected pO_2 until a steady value was observed. Measurements were made in air initially, then the pO_2 steadily reduced until the final measurement was made in hydrogen, after which the sample was allowed to cool down in the reducing atmosphere. Fracture surfaces of the bar samples were then examined in SEM.

3 Results

3.1 Sintering studies

Linear shrinkage versus temperature data obtained during the sintering of green powder compacts of nominal compositions $La_{1-x}Ca_xCr_{0.9}Ni_{0.1}O_3$ where x = 0·2, 0·3 and 0·4 are compared with shrinkage data for a pellet of composition $La_{0.8}Ca_{0.2}CrO_3$ as shown in Fig 1. Virtually no shrinkage between room temperature and 1550°C is seen for $La_{0.8}Ca_{0.2}CrO_3$. The compositions for which 10 mol% of the chromium had been substituted by nickel all commence shrinking at just above 1000°C and it can be seen that as the calcium level is increased in the nickel doped compounds a given percentage of linear shrinkage is attained at progressively lower temperatures. By 1550°C the total linear shrinkage for the sample of composition $La_{0.8}Ca_{0.2}Cr_{0.9}Ni_{0.1}O_3$ was 8·6% and

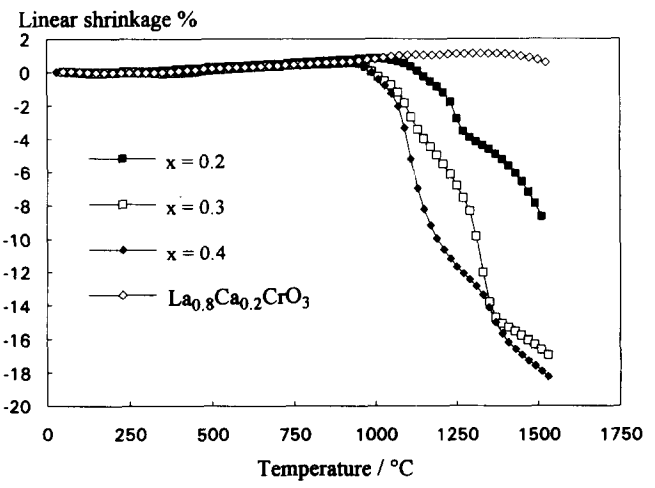

Fig. 1. Linear shrinkage versus temperature for $La_{0.8}Ca_{0.2}CrO_3$ and $La_{1-x}Ca_xCr_{0.9}Ni_{0.1}O_3$.

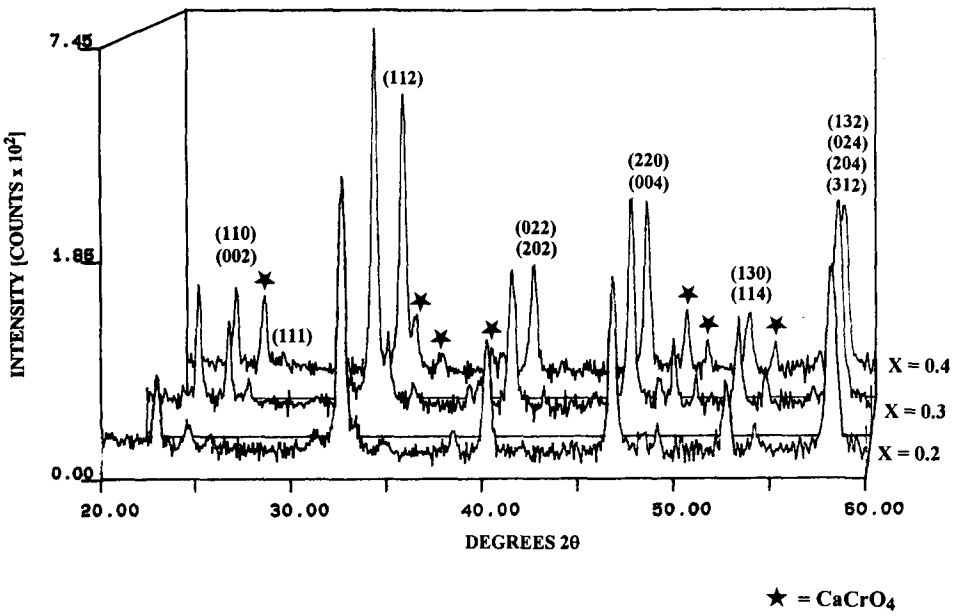

Fig. 2. XRD analysis of $La_{1-x}Ca_xCr_{0.9}Ni_{0.1}O_3$ calcined powder.

for samples of compositions $La_{0.7}Ca_{0.3}Cr_{0.9}Ni_{0.1}O_3$ and $La_{0.6}Ca_{0.4}Cr_{0.9}Ni_{0.1}O_3$, 16·93% and 18·25%, respectively. One can therefore say that for the nickel substituted compositions, increasing the calcium level increases the sinterability of the system, without the nickel substitution no densification takes place. There is an inflection in the sintering curve of $La_{0.8}Ca_{0.2}Cr_{0.9}Ni_{0.1}O_3$ at 1290°C and in the sintering curves of $La_{0.7}Ca_{0.3}Cr_{0.9}Ni_{0.1}O_3$ and $La_{0.6}Ca_{0.4}Cr_{0.9}Ni_{0.1}O_3$ at 1370°C. Inflections in sintering curves suggest a change in the sintering mechanism at that point. Mass transport is achieved much more readily in the liquid state than the solid state and pronounced curvature of the shrinkage data is usually an indication that the sintering proceeded by the generation of liquid phases.

XRD analysis was carried out for all three compositions on both powder and bulk ceramic specimens. Figures 2 and 3 show the diffraction traces obtained for powder and sintered ceramic respectively. Reflections from the perovskite are indexed to the orthorhombic $La_{1-x}Ca_xCrO_3$ system. The XRD results prove that the calcium and nickel doped powders under investigation did not consist entirely of the perovskite phase, but contained significant amounts of $CaCrO_4$. The ratio of the relative intensity of the $CaCrO_4$ peaks to the perovskite peaks increased with the level of calcium substitution in the powders. The sintered ceramic however proved to be predominantly single phase perovskite. There were a few small extraneous reflections in the trace from the sintered ceramic just above the background level, which may correspond to residual $CaCrO_4$ or $Ca_5(CrO_4)_3OH$. The $Ca_5(CrO_4)_3OH$ phase has been reported as sometimes being present on the surface of chromium deficient calcium doped lanthanum chromite.[23]

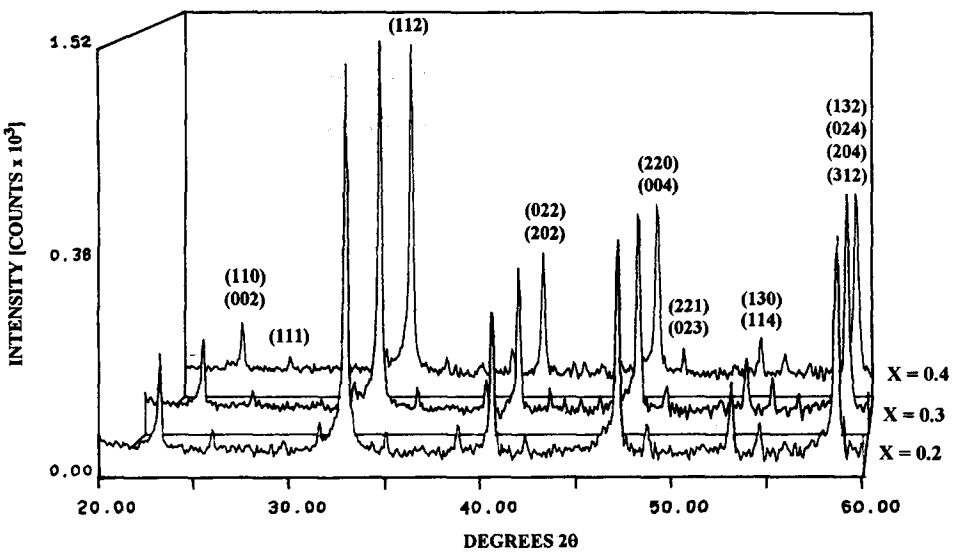

Fig. 3. XRD analysis of $La_{1-x}Ca_xCr_{0.9}Ni_{0.1}O_3$ sintered ceramic.

Table 1. Lattice parameters, unit cell volumes and calculated theoretical densities for (La, Ca)$Cr_{0.9}Ni_{0.1}O_3$

Mol % calcium	a (Å ±0·001)	b (Å ±0·001)	c (Å ±0·001)	Cell volume ($Å^3$)	XRD density (g/cm^3)
20	5·4405	5·4222	7·7062	227·33	6·421
30	5·4240	5·4110	7·6877	225·63	6·179
40	5·4094	5·3993	7·6494	223·41	5·946

The XRD results from the sintered ceramic were also used to calculate unit cell lattice parameters hence theoretical densities for the compounds were obtained. The results are summarised in Table 1. After 5 h at a furnace temperature of 1500°C the sample of composition $La_{0.8}Ca_{0.2}Cr_{0.9}Ni_{0.1}O_3$ had sintered to 96% of the theoretical density calculated by XRD and samples of composition $La_{0.7}Ca_{0.3}Cr_{0.9}Ni_{0.1}O_3$ and $La_{0.6}Ca_{0.4}Cr_{0.9}Ni_{0.1}O_3$ both sintered to 98% theoretical density.

Quench studies confirmed that liquids were being generated in the system during the sintering regime. Microstructures of the quenched samples are shown in Figs 4–7. Figures 4 and 5 are fracture surfaces of $La_{0.7}Ca_{0.3}Cr_{0.9}Ni_{0.1}O_3$ quenched from 1170°C and 1385°C, respectively. Large areas of a phase that would have been liquid at 1170°C, appearing dark in backscattered electron mode are well contrasted by the lighter grey matrix of the perovskite in Fig. 4. Figure 5 reveals similar areas of quenched liquid which appear lighter in the secondary electron image, the micrographs were taken at the same magnification. Less liquid and increased grain growth of the matrix can be seen in the sample quenched from the higher temperature.

Figures 6 and 7 are micrographs of the actual surfaces of a pellet of composition $La_{0.6}Ca_{0.4}Cr_{0.9}Ni_{0.1}O_3$ quenched from 1170°C. Figure 6, taken in backscattered electron mode shows the dark liquid

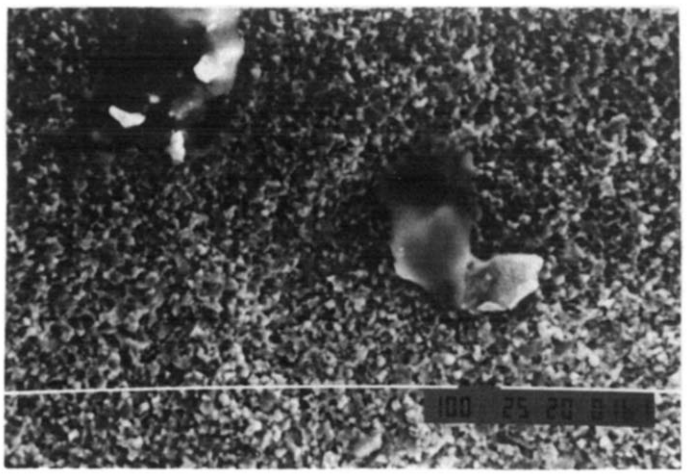

Fig. 5. Fracture surface of $La_{0.7}Ca_{0.3}Cr_{0.9}Ni_{0.1}O_3$ quenched from 1385°C during sintering. Secondary electron image. Magnification ×750; bar, 100 μm.

oozing out of pores and then presumably as a result of the air cool, crystallising out across the surface of the pellet. Figure 7 is a lower magnification micrograph of the same sample. It is evident that the volume of liquid generated at this temperature, is very substantial in this composition which contains the highest level of calcium. The result of EDAX analysis of the large dark areas of quenched liquid in Figs 6 and 7 is shown in Fig. 8. It can be seen that the characteristic X-ray radiation was predominantly from calcium and chromium.

SEM micrographs of polished thermally etched surfaces and fractured thermally etched surfaces of fully sintered ceramic are shown in Figs 9 and 10 respectively. It can be seen that the samples have sintered to high density with a fine regular grain structure and showing no evidence of residual liquid phase.

The results of the DTA analysis on powders of nominal composition $La_{0.8}Ca_{0.2}Cr_{0.9}Ni_{0.1}O_3$ and $La_{0.7}Ca_{0.3}Cr_{0.9}Ni_{0.1}O_3$ are displayed in Fig. 11. For

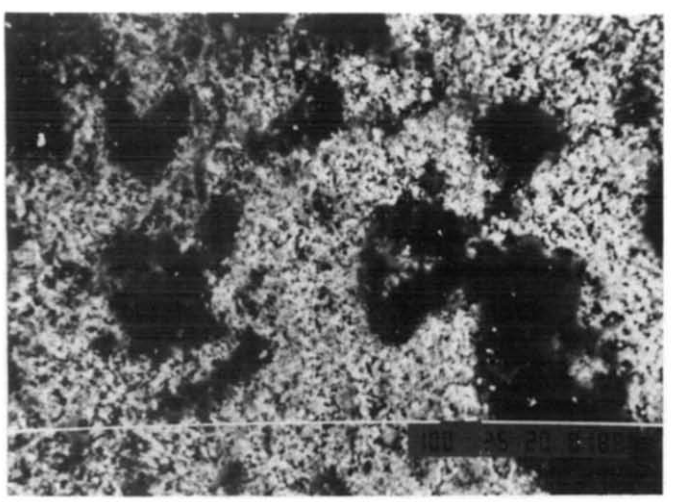

Fig. 4. Fractured surface of $La_{0.7}Ca_{0.3}Cr_{0.9}Ni_{0.1}O_3$ quenched from 1170°C during sintering. Backscattered electron image. Magnification ×750; bar, 100 μm.

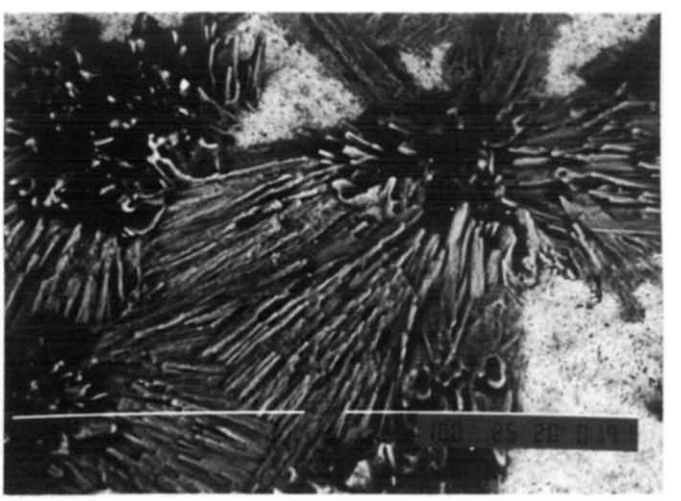

Fig. 6. Surface of $La_{0.6}Ca_{0.4}Cr_{0.9}Ni_{0.1}O_3$ quenched from 1170°C during sintering. Backscattered electron image. Magnification ×500; bar, 100 μm.

Fig. 7. Surface of $La_{0.6}Ca_{0.4}Cr_{0.9}Ni_{0.1}O_3$ quenched from 1170°C during sintering. Backscattered electron image. Magnification ×75; bar, 1000 μm.

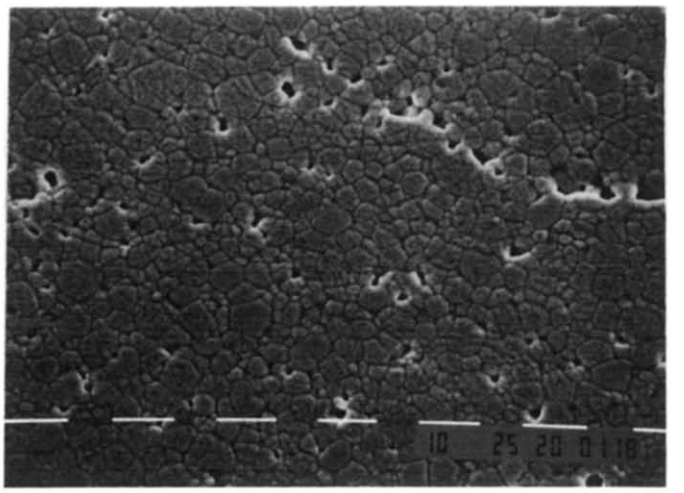

Fig. 9. Polished and thermally etched surface of $La_{0.8}Ca_{0.2}Cr_{0.9}Ni_{0.1}O_3$, sintered 1500°C, 5 h. Secondary electron image. Magnification ×1000; bar, 10 μm.

both compositions large exothermic reactions peaking at 1065°C were noted. The exothermic reaction was stronger in the compound which contained a higher level of calcium substitution.

(TEM) Transmission electron micrographs of the sample of composition $La_{0.7}Ca_{0.3}$-$Cr_{0.9}Ni_{0.1}O_3$ are shown in Figs 12 and 13. Figure 12 shows residual second phase material remaining at a triple point after sintering. Likewise, Fig. 13 shows a similar second phase material remaining at the boundary between two of the perovskite grains. Further investigation of this phase was made by semi-quantitative EDAX analysis. For the second phase in Fig. 12 the EDAX analysis was done with the microscope in TEM mode, whereas for Fig. 13, EDAX analysis was done with the microscope in STEM mode with a very fine, (~100 Å) intense beam. As a result of using such a beam, a contamination cone in Fig. 13 can be seen to have been built up at the point on the second phase where the analysis was performed. EDAX analyses of the matrix and the intergranular phase are shown in Figs 14 and 15, indicating that the main phase, appearing darker in the transmitted light, is the perovskite and the lighter coloured second phase consisted again almost entirely of calcium and chromium. From semi-quantitative chemical analysis, the calcium to chromium ratio in the second phase material was found to be approximately 1 : 1. It was concluded that residual $CaCrO_4$, not visible in SEM, remained at grain boundaries and triple points after sintering.

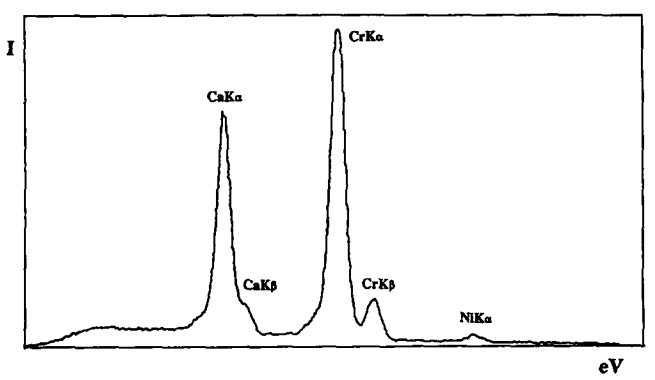

Fig. 8. EDAX analysis of the quenched liquid in Figs 6 and 7.

3.2 Chemical stability in hydrogen

Following a 200 h anneal at 900°C in wet forming gas, sintered ceramic of composition $La_{0.8}Ca_{0.2}$-$Cr_{0.9}Ni_{0.1}O_3$ was analysed by XRD and SEM. No evidence for the dissolution of Ni from the solid solution was provided by XRD. Figure 16 shows a backscattered scanning electron micrograph of the fracture surface of the reduced ceramic, the microstructure appears to have remained intact and there is no visible Ni precipitation. However when the reduced ceramic was polished and thermally etched prior to examination in SEM, the instability of the compound became apparent, Fig. 17. During the thermal etch in air, the fine Ni

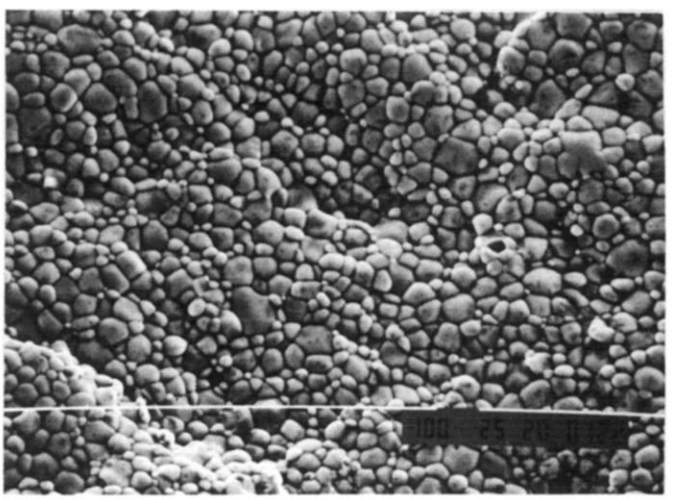

Fig. 10. Fractured and thermally etched surface of $La_{0.8}Ca_{0.2}Cr_{0.9}Ni_{0.1}O_3$, sintered 1500°C, 5 h. Secondary electron image. Magnification ×750; bar, 100 μm.

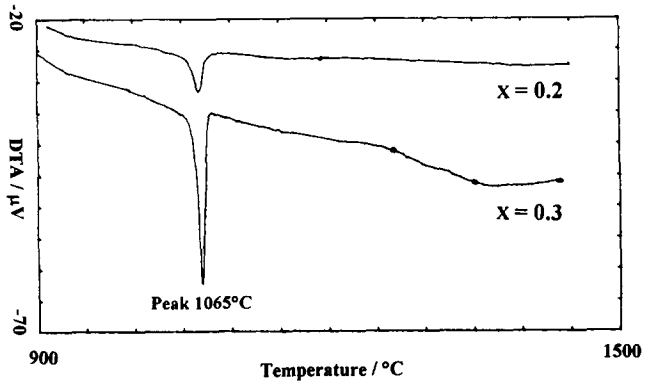

Fig. 11. DTA analysis $La_{1-x}Ca_xCr_{0.9}Ni_{0.1}O_3$, powders.

precipitates which would have been formed during the reduction have oxidised and grown and can now be clearly observed at grain boundaries and triple points. The results are consistent with the work of Koc and Anderson[16] and Milliken *et al.*[24] who independently report that the precipitation of Co from reduced $La_{1-x}Ca_xCr_{1-y}Co_yO_3$ ceramic could not be detected by XRD.

3.3 Electrical conductivity

Electrical conductivity data at 1000°C, is presented as a function of oxygen partial pressure in Fig. 18. The sample of composition $La_{0.8}Ca_{0.2}Cr_{0.9}Ni_{0.1}O_3$ had a conductivity of 45 S/cm in air and seemed to follow the classical model for *p*-type oxides. The data for this composition shows a region of relatively stable conductivity where compensation for the introduction Ca^{2+} ions results in the formation of small polarons as charge carriers and then transfers to a region of falling conductivity where the predominant compensation mechanism for the lower valence cations changes from electronic to ionic, resulting in the formation of oxygen vacancies. The sample of composition $La_{0.7}Ca_{0.3}Cr_{0.9}Ni_{0.1}O_3$ had a conductivity of 61 S/cm in air, but deviations from the defect model were apparent in the pO_2 range 10^{-3}–10^{-7} atm, where

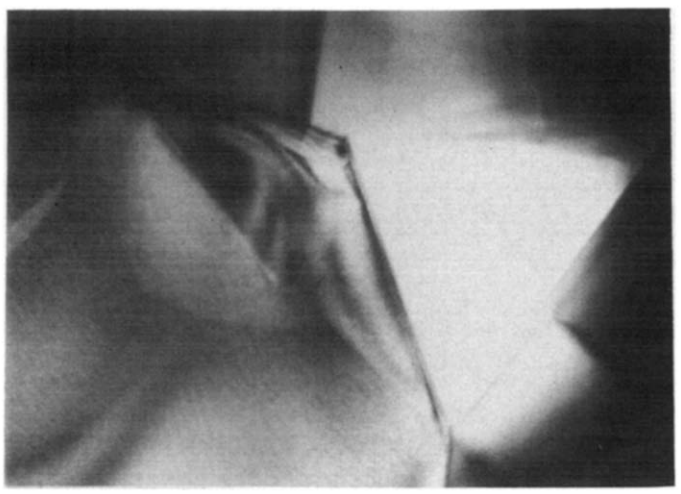

Fig. 12. TEM micrograph of $La_{0.7}Ca_{0.3}Cr_{0.9}Ni_{0.1}O_3$ sintered ceramic. Second phase at triple point. Magnification ×26000.

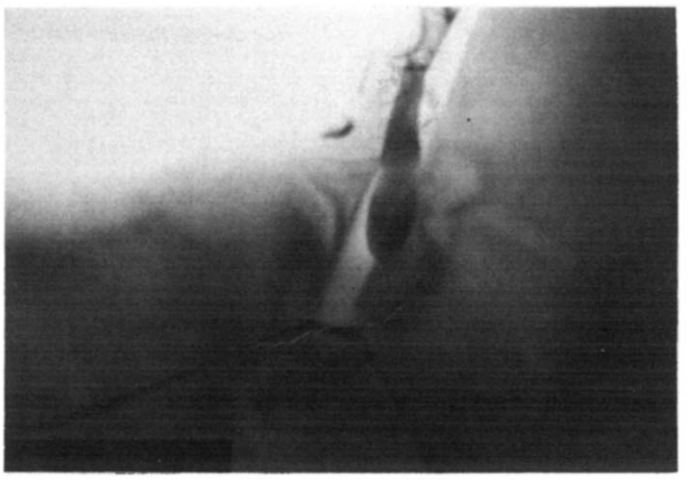

Fig. 13. TEM micrograph of $La_{0.7}Ca_{0.3}Cr_{0.9}Ni_{0.1}O_3$ sintered ceramic. Second phase at grain boundary. Magnification ×50000.

the conductivity was lower than expected. On cooling, the bar sample was found to be cracked and embrittled. The sample of composition $La_{0.6}Ca_{0.4}Cr_{0.9}Ni_{0.1}O_3$ had a conductivity of 92 S/cm in air. During the course of experiment the sample became severely unstable, exhibiting large deviations from the model, particularly at a pO_2 of $10^{-7.5}$ atm where the conductivity rose to over 200 S/cm. The test was aborted at a pO_2 of $10^{-11.5}$ atm as the measured voltage signal became very noisy. As for the previous composition, on cooling the sample was found to be cracked and embrittled.

On completion of the tests, all compositions were cooled in a reducing atmosphere and fractured surfaces of the bar samples were examined in SEM. Figures 19 and 20 show secondary electron micrographs of the fracture surfaces of the samples of composition $La_{0.7}Ca_{0.3}Cr_{0.9}Ni_{0.1}O_3$ and $La_{0.6}Ca_{0.4}Cr_{0.9}Ni_{0.1}O_3$, respectively. It is quite clear that the conditions experienced during these experiments were aggressive enough to induce instability and severe microstructural degradation of the samples. Similar degradation was observed in the sample of composition $La_{0.8}Ca_{0.2}Cr_{0.9}Ni_{0.1}O_3$ but the degradation became more extensive as the

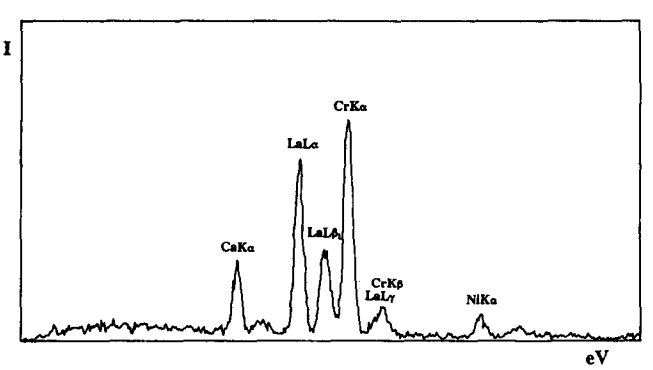

Fig. 14. EDAX analysis of the perovskite phase in Figs 12 and 13.

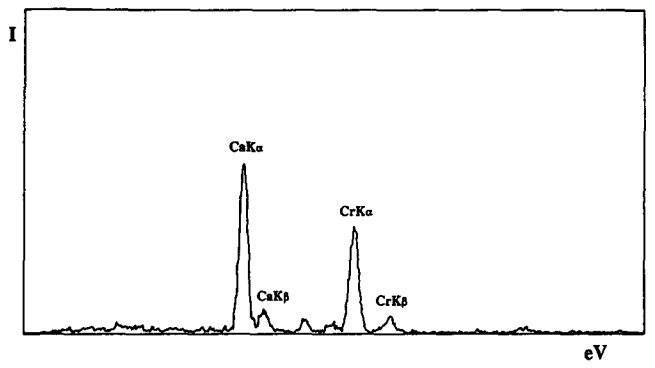

Fig. 15. EDAX analysis of the intergranular phase in Figs 12 and 13.

level of calcium substitution within the system increased; this is consistent with the knowledge that deviations from model conductivity behaviour also became more pronounced as the calcium level was increased. The regular grain structure of the 'as-sintered' samples depicted in Figs 9 and 10 has been broken down and microstructures now contain a large amount of porosity. Fracture surfaces no longer show intergranular fracture but it seems

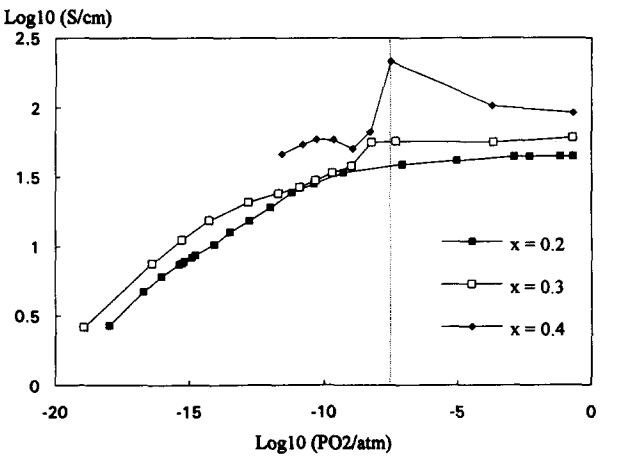

Fig. 18. Electrical conductivity as a function of pO_2 for $La_{1-x}Ca_xCr_{0.9}Ni_{0.1}O_3$.

as though liquids have been regenerated and quenched into the microstructure on cooling, this has resulted in a change in the fracture mechanism and serious embrittlement of the samples. In the sample of composition $La_{0.6}Ca_{0.4}Cr_{0.9}Ni_{0.1}O_3$ the degradation is very severe, large pores have devel-

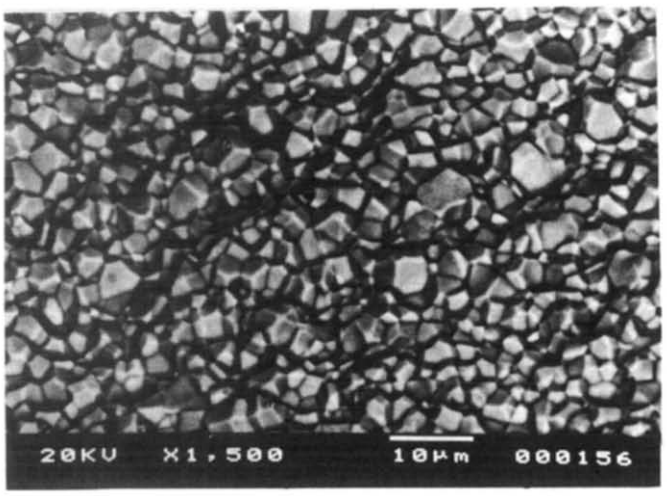

Fig. 16. Fracture surface of $La_{0.8}Ca_{0.2}Cr_{0.9}Ni_{0.1}O_3$, reduced 5×10^{-16} atm, 900°C, 200 h. Backscattered electron image. Magnification ×1500; bar, 10 μm.

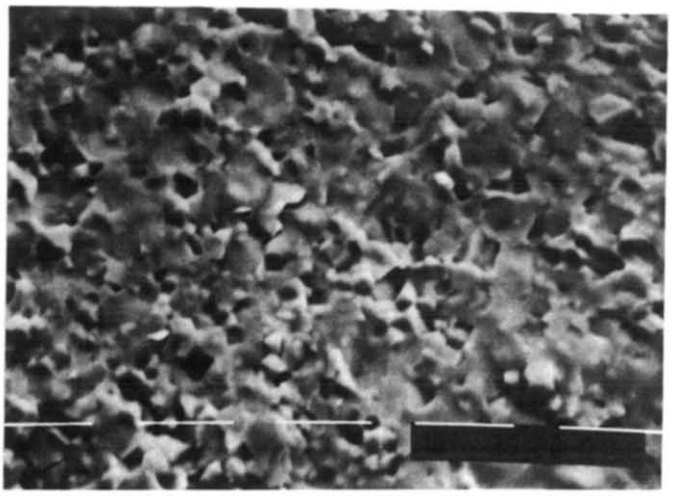

Fig. 19. Fracture surface of $La_{0.7}Ca_{0.3}Cr_{0.9}Ni_{0.1}O_3$ bar sample on completion of the electrical conductivity experiment. Secondary electron image. Magnification ×1500; bar, 10 μm.

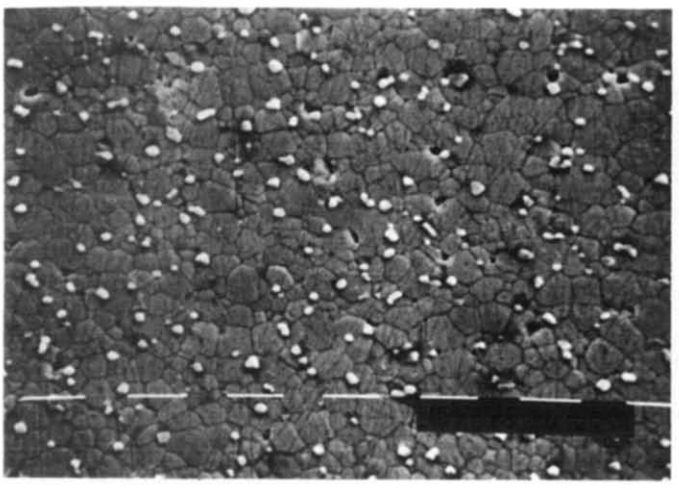

Fig. 17. Fracture surface of $La_{0.7}Ca_{0.3}Cr_{0.9}Ni_{0.1}O_3$, reduced 5×10^{-16} atm, 900°C, 200 h. Secondary electron image. Magnification ×1000; bar, 10 μm.

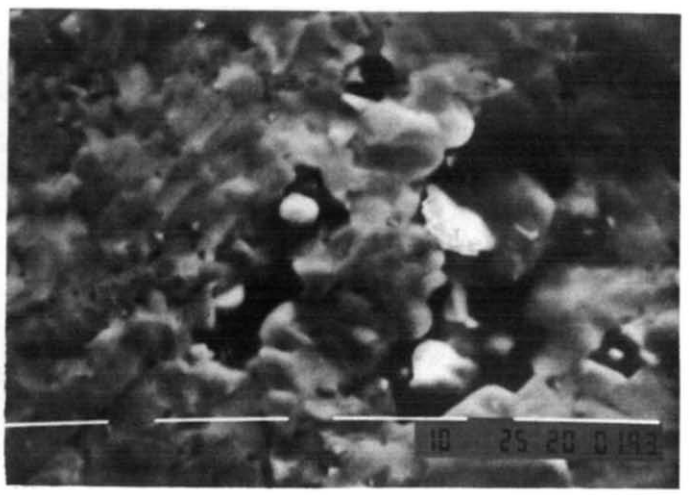

Fig. 20. Fracture surface of $La_{0.6}Ca_{0.4}Cr_{0.9}Ni_{0.1}O_3$ bar sample on completion of the electrical conductivity experiment. Secondary electron image. Magnification ×2000; bar, 10 μm.

oped and the nickel has also come out of solid solution. A sample of composition $La_{0.6}Ca_{0.4}Cr_{0.9}Ni_{0.1}O_3$ was simply placed in the chamber during one of experiments. The sample was exposed to the same range in oxygen partial pressure as the actual bar samples used in the conductivity experiment, but no current was passed through the specimen. The degradation was found to be just as extensive in this sample as it was in the actual test sample and therefore any possibility of the electric current exerting an influence on the degradation processes can be eliminated.

4 Discussion

4.1 Sintering studies

The liquid phases that were frozen into the microstructures of the samples which had been quenched from moderate temperatures during the sintering regime are believed to facilitate densification of the compounds. In order to cause densification there should be an appreciable amount of liquid phase, coupled with solubility of the solid in the liquid and wetting of the solid by the liquid. If these conditions are satisfied the liquid increases the rate of mass transport during sintering by solution and reprecipitation of solids leading to particle rearrangement and grain growth. Liquid phase sintering is usually a two stage process involving particle rearrangement followed by pore elimination via viscous flow of liquid at grain boundaries, and the driving force for densification is derived from the capillary pressure of the liquid phase located between the fine solid particles.

A significant amount of $CaCrO_4$ was present as a second phase in the $La_{1-x}Ca_xCr_{0.9}Ni_{0.1}O_3$ powders. The temperature of the endothermic reaction in the DTA results from $La_{0.8}Ca_{0.2}Cr_{0.9}Ni_{0.1}O_3$ and $La_{0.7}Ca_{0.3}Cr_{0.9}Ni_{0.1}O_3$ powders coincides well with the onset of densification in the shrinkage curves and it is therefore reasonable to assume that the liquids were formed by the decomposition of the $CaCrO_4$ second phase in the powders.

The most recent phase relations in the CaO–Cr_2O_3 binary system were established by deVilliers *et al.* in 1987 and are reproduced in Fig. 21.[25] According to their diagram, stoichiometric $CaCrO_4$ is stable from room temperature to 1073 ± 3°C when it melts incongruently to form β-$CaCr_2O_4$ and liquid. With increasing temperature the composition of the liquid will change until approximately 1340°C when the system will become entirely liquid. In a recent paper[23] Sakai and co-workers discuss the phase relationships in the CaO-Cr_2O_3 system with reference to their calculated phase diagram which is in disagreement with the experimental one by deVilliers. There is a

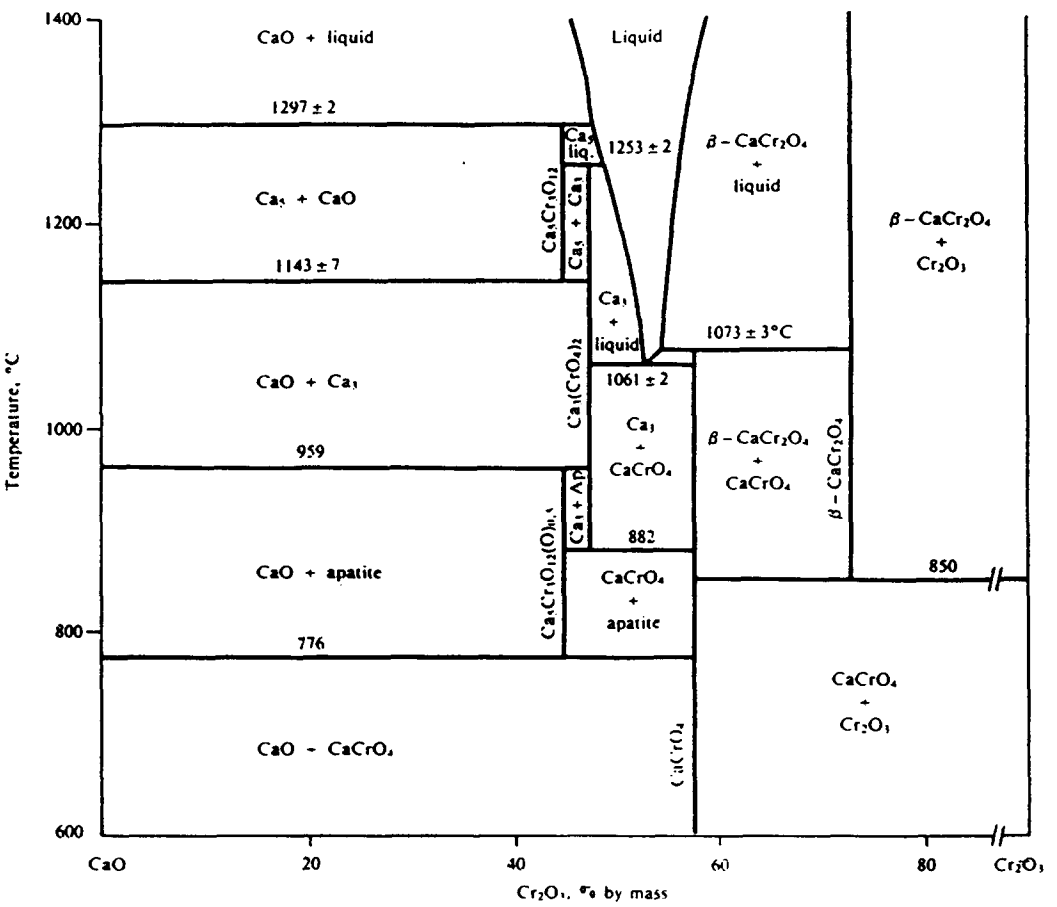

Fig. 21. CaO–Cr_2O_3 binary phase diagram in air. From Ref. 25, reproduced by permission.

eutectic on the calcium rich side of $CaCrO_4$ at 1061 ± 2°C, therefore if the $CaCrO_4$ phase in the powders is slightly calcium rich one would expect the formation of liquid at 1061°C, before entering the β-$CaCr_2O_4$ and liquid phase field at 1073°C. The observation that an endothermic reaction in the DTA experiment peaked at 1065°C suggests that the $CaCrO_4$ phase in the $La_{1-x}Ca_xCr_{0.9}Ni_{0.1}O_3$ powder is therefore slightly calcium rich.

The inflections in the sintering curves of $La_{0.7}Ca_{0.3}Cr_{0.9}Ni_{0.1}O_3$ and $La_{0.6}Ca_{0.4}Cr_{0.9}Ni_{0.1}O_3$ at 1370°C correspond to a change in the sintering mechanism at this temperature. They also coincide well with the dissolution of the β-$CaCr_2O_4$ phase into the liquid, predicted to occur at approximately 1340°C by the CaO–Cr_2O_3 phase diagram. By contrast, the inflection in the sintering curve of $La_{0.7}Ca_{0.3}Cr_{0.9}Ni_{0.1}O_3$ occurred at 1290°C and is not well explained by the phase diagram. Since less liquid will have been formed in this composition and it is possible that all of the liquid will have dissolved into the solid solution with the perovskite before this temperature was reached.

Less liquid was noted in samples quenched from 1385°C than in those quenched from 1170°C and no evidence of residual liquid phase can be seen in SEM micrographs (Figs 9 and 10) of fully sintered ceramic. The liquid phase is therefore considered to be transient. The TEM results, however, proved that the liquid was not truly transient, since small amounts of residual $CaCrO_4$, not visible in SEM, remained at grain boundaries and triple points after sintering.

4.2 Electrical conductivity

Substantial chemical and microstructural degradation occurred in the $La_{1-x}Ca_xCr_{0.9}Ni_{0.1}O_3$ system when exposed to an atmosphere containing a mixture of CO_2 and H_2 (forming gas) at a temperature of 1000°C. Microstructural analysis of reduced samples indicate that under these conditions liquids could have been regenerated. The substantial increase in electrical conductivity in the sample of composition $La_{0.6}Ca_{0.4}Cr_{0.9}Ni_{0.1}O_3$ at a pO_2 of $10^{-7.5}$ atm is further evidence for microstructural changes.

The simple explanation for degradation is to attribute it entirely to the precipitation of nickel from solid solution in the perovskite that was observed during hydrogen stability tests. The dissolution of nickel will certainly account for a great deal of the degradation observed in CO_2 and H_2 atmospheres during conductivity tests but the following facts lead one to suspect that the degradation process is more complex. The degradation observed in the H_2 stability experiment was minimal, the bulk microstructure appeared to have remained intact following the reduction and the nickel dissolution only became apparent when the reduced material was thermally etched. In contrast, the degradation in CO_2 and H_2 containing atmospheres during electrical conductivity experiments was very pronounced and samples actually disintegrated. Also, the degradation in the conductivity experiment became more pronounced as the level of calcium substitution within the compounds was increased, all compounds contained the same level of nickel substitution therefore one would expect the same amount of degradation in all the compounds if the nickel had been purely responsible for the instability. It should be noted that the initial hydrogen stability tests were performed at 900°C whereas the conductivity measurements were carried out at 1000°C, however the fact that a mixture of gases was used during the conductivity experiment may have an influence on the severity of the degradation.

4.3 Chemical stability of $CaCrO_4$

A possible cause of the increased degradation observed in the electrical conductivity experiments is a chemical reaction involving both H_2 and CO_2 with the residual $CaCrO_4$ observed at the grain boundaries and triple points in $(La,Ca)Cr_{0.9}Ni_{0.1}O_3$. It was therefore necessary to establish whether or not $CaCrO_4$ reacts with the gas mixtures used, and if so to quantify the reactions.

$CaCrO_4$ powder was prepared by the citrate route and confirmed to be phase pure by XRD. DTA/TG analysis was then performed on the $CaCrO_4$ powder in atmospheres of CO_2 and forming gas, (90% N_2, 10% H_2). The gas flow rate through the chamber was restricted to 70 ml/min. The temperature range over which data was collected from 20°C to 1000°C and 1200°C. After each experiment reaction products were analysed by XRD. The heating rate used in the experiments was 10°C/min.

In 1976 Pánek and Kanclír published phase relations in the CaO–Cr_2O_3 system at a pO_2 of 10^{-6} atm, which are reproduced in Fig. 22.[26] Whereas the phase diagram in air shows $CaCrO_4$ to be stable up to its melting temperature of 1073°C, the diagram at reduced pO_2 shows $CaCrO_4$ decomposing at around 750°C to form $Ca_9Cr_6O_{24}$, and $Ca_6Cr_{12}O_{27}$. Pánek then proposed a phase field extending from around 820°C to 1000°C in which the $Ca_6Cr_{12}O_{27}$ and CaO phases are stable. Above 1000°C, at a pO_2 of 10^{-6} atm, Pánek proposed a phase field in which the β-$CaCr_2O_4$ and CaO phases are stable. The phase $Ca_6Cr_{12}O_{27}$ cannot be found in the ASTM index but Pánek listed interplanar distances and relative intensities for this phase in his published work.

Figure 23 shows our DTA/TG results for

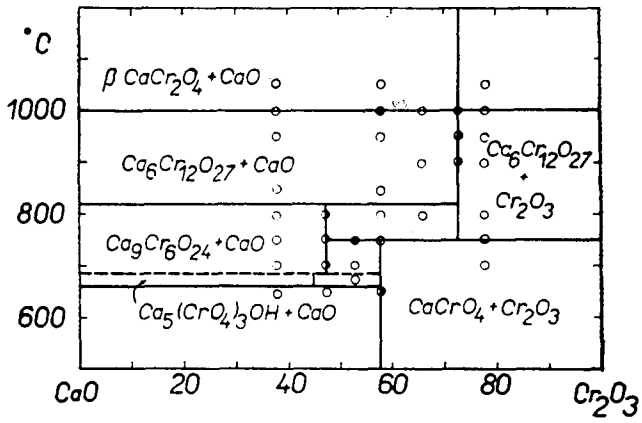

Fig. 22. CaO–Cr_2O_3 binary phase diagram in $pO_2 \approx 10^{-6}$ atm and $pH_2O \approx 10^{-7}$ atm. From Ref. 26, reproduced by permission.

$CaCrO_4$ exposed to an atmosphere of forming gas. The DTA trace shows a large exothermic reaction peaking at 640°C, and the corresponding TG results show a weight loss of 14·76% associated with this reaction. No other reactions were registered. XRD analysis showed that the reaction products consisted entirely of CaO and the complex oxychromite phases: $Ca_9Cr_6O_{24}$ and $Ca_6Cr_{12}O_{27}$. No reflections from residual $CaCrO_4$ were detected.

The DTA/TG results from the experiment in CO_2 are presented in Fig. 24. A broad endotherm commences at around 850°C, peaks at 1020°C and reaches completion shortly afterwards. TG results showed an 8·8% weight loss associated with this reaction. Another smaller endothermic peak was observed at around 1130°C, and a further 2·6% weight loss associated with this reaction. It is obvious from the TG results that this reaction also occurred over a range in temperature. From XRD analysis of the reaction products at 1000°C, five phases were identified. As in the case of H_2 exposure, CaO, $Ca_9Cr_6O_{24}$ and $Ca_6Cr_{12}O_{27}$ phases could all be indexed, but significant amounts of $CaCO_3$ and unreacted $CaCrO_4$ were also detected. The intensity of the reflections from CaO were much weaker than they were in the reaction products from the H_2 experiment. From XRD analysis of the reaction products at 1200°C, CaO, $Ca_9Cr_6O_{24}$, $Ca_6Cr_{12}O_{27}$ and β-$CaCr_2O_4$ phases

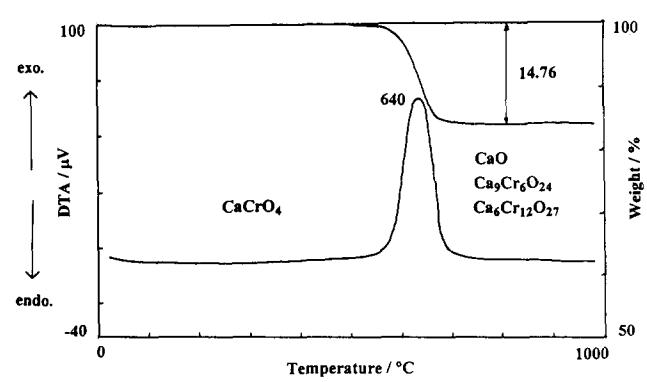

Fig. 23. DTA/TG analysis of $CaCrO_4$ powder in (90/10) N_2/H_2.

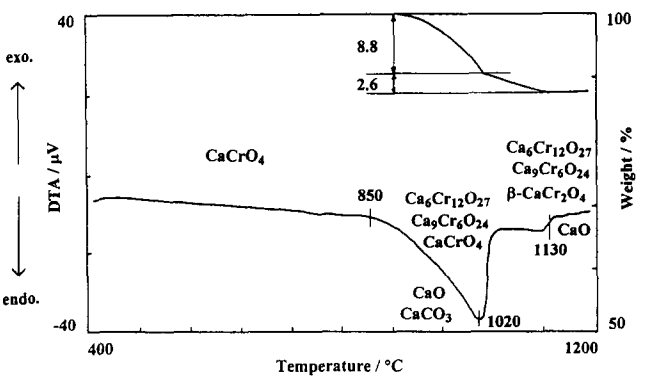

Fig. 24. DTA/TG analysis of $CaCrO_4$ powder in CO_2.

could all be indexed, the reflections from CaO being much stronger than they were in the reaction products at 1000°C. Owing to the large number of phases there were many overlapping peaks in the reaction products from the high temperature CO_2 experiment which made the results difficult to interpret. Residual $CaCO_3$ and $CaCrO_4$ peaks may also have been present just above background level in the XRD pattern.

The results of the hydrogen experiment agree very well with Pánek's data.[26] The reaction products consisted only of $Ca_9Cr_6O_{24}$, $Ca_6Cr_{12}O_{27}$ and CaO phases. In the CO_2 experiment the broad endothermic reaction from 850 to 1020°C is thought to correspond to the decomposition of $CaCrO_4$ and the formation of $Ca_9Cr_6O_{24}$, $Ca_6Cr_{12}O_{27}$ and CaO phases. Over this temperature range the CaO formed will react with CO_2 to form $CaCO_3$. The smaller broad endothermic reaction at higher temperature is thought to correspond to the decomposition of $CaCO_3$ and the formation of the high temperature β-$CaCr_2O_4$ phase.

The results are similar to those published by Kashihara and co-workers[27] who used DTA/TG to study the decomposition of $CaCrO_4$ in CO and H_2 atmospheres. A single large exothermic peak was reported for H_2, with reaction products including CaO and a complex oxychromite phase the authors could not index and simply termed α-phase. By contrast under CO the intermediate reaction was exothermic, not endothermic, but the reaction products were still consistent with the ones reported here. Also in the CO case, the authors noted the formation of CaO and subsequent formation and decomposition of $CaCO_3$.

The $CaCrO_4$ decomposed at progressively lower temperatures as the pO_2 was reduced. In air $CaCrO_4$ decomposes at 1073°C to β-$CaCr_2O_4$ and liquid. In CO_2 the $CaCrO_4$ decomposed at around 850°C and formed the intermediate phases $Ca_9Cr_6O_{24}$ $Ca_6Cr_{12}O_{27}$ CaO and $CaCO_3$ before the formation of β-$CaCr_2O_4$. In H_2, $CaCrO_4$ decomposed at around 640°C again forming the inter-

mediate phases $Ca_9Cr_6O_{24}$ $Ca_6Cr_{12}O_{27}$ and large amounts of CaO.

Degradation of $(La,Ca)Cr_{0.9}Ni_{0.1}O_3$ was much more severe in hydrogen, carbon dioxide gas mixtures than it was in hydrogen forming gas alone. It is thought that in H_2 + CO_2 gas mixtures the hydrogen content catalyses a surface reaction to form CaO which subsequently reacts with CO_2 to form $CaCO_3$.

5 Summary and Conclusion

The substitution of 10 mol% Ni for Cr in Ca doped $LaCrO_3$ results in the precipitation of $CaCrO_4$ second phase material in calcined powders. The second phase melts at 1060–1070°C resulting in the generation of Ca- and Cr-rich liquid which changes composition with temperature. The liquid promotes mass transport and densification of the compound, but becomes itself soluble within the perovskite $LaCrO_3$ grains at high temperature. The liquid phase is therefore transient. Compositions in the system achieved 96–98% of theoretical density after 5 h at 1500°C and it is thought that closed porosity could be achieved at lower temperatures. The system however has been shown to become unstable in hydrogen atmospheres due to the dissolution of nickel from the solid solution. Electrical conductivity at 1000°C in air was high, 92 S/cm for a 40 mol% calcium substitution, but during the electrical conductivity experiments serious microstructural degradation occurred in mixtures of CO_2 and hydrogen. It is shown that residual $CaCrO_4$ remains at grain boundaries and triple points after sintering and in addition to nickel dissolution, $CaCrO_4$ is not stable in CO_2 and H_2 atmospheres. The $CaCrO_4$ decomposes to form complex calcium oxychromate phases and CaO. CO_2 then reacts with the CaO to form $CaCO_3$, H_2 acts as a catalyst for this reaction by increasing the amount of CaO formed.

The $(La,Ca)Cr_{0.9}Ni_{0.1}O_3$ system would not be chemically and mechanically stable as an interconnect material in a solid oxide fuel cell. The work brings the stability of all liquid phase sintered Ca doped lanthanum chromites into question and emphasises the need for thorough stability tests before liquid phase sintered Ca doped lanthanum chromites are incorporated into the fuel cell stacks.

Acknowledgements

Financial support of the UK Science and Engineering Council, ICI Advanced Materials and Tioxide UK is gratefully acknowledged as is the technical assistance of Mr G. Dolman of ICI and Mr G. Briers of Imperial College.

References

1. Hooie, D. T., Status of SOFC development in USA. *Proc. 3rd Int. Symposium on SOFC'S*, eds S. C. Singhal & H. Iwahara. The Electrochemical Society, Pennington, NJ, USA, pp. 3–5.
2. Zegers, P., Status of SOFC development in Europe. In *Proc. 3rd Int. symposium on SOFC's*, eds S. C. Singhal & H. Iwahara. The Electrochemical Society, Pennington, NJ, USA, pp. 16–20.
3. Yasuda, I. & Hikita, T., Electrical conductivity and defect structure of calcium doped lanthanum chromite. *J. Electrochem. Soc.*, **140**(6) (1993) 1699–704.
4. Karim, D. P. & Aldred, A. T., Localized level hopping in $La(Sr)CrO_3$. *Phys. Rev. B*, **20** (1979) 2255–63.
5. Flandermeyer, B. F., Nasrallah, M. M., Sparlin, D. M. & Anderson, H. U., High temperature stability of magnesium doped lanthanum chromite. *High Temp. Sci.*, **20** (1985) 259–69.
6. Richards, V. L. & Singhal, S. C., Method of making highly sinterable lanthanum chromite powder, European Patent 0447 717 A1, Westinghouse Electric Corp., 1991.
7. Yokokawa, H., Sakai, N., Kawada, T. & Dokiya, M., Chemical thermodynamic considerations in sintering of $LaCrO_3$ based perovskites. *J. Electrochem. Soc.*, **138**(4) (1991) 1018–27.
8. Groupp, L. & Anderson, H. U., Densification of $La_{1-X}Sr_XCrO_3$. *J. Am. Ceram. Soc.*, **59**(9–10) (1976) 449–50.
9. Flandermeyer, B. K., Dusek, J. T., Blackburn, P. E. Dees, D. W., McPheeters, C. C. & Poeppel, R. B., Addition of 8–10 wt.% of a (La or Y)-Mg fluoride mixture as a sintering aid. *Abstracts of the 1986 Fuel Cell Seminar*, Courtesy Associates Inc., Washington, DC, USA, 1986, pp. 68–71.
10. Flandermeyer, B. K. *et al.*, Sintering aid for lanthanum chromite refractories, US Patent 4,749,632, June 1988.
11. Meadowcroft, D. B., Some properties of strontium-doped lanthanum chromite. *Br. J. Appl. Phys. (J. Phys. D.)*, **2**(2) (1969) 1225–33.
12. Bansal, K. P., Kumari, S., Das, B. K. & Jain, G. C., On the sintering and dielectric properties of ceramic $La_{0.96}Sr_{0.04}CrO_3$. *Trans. J. Br. Ceram. Soc.*, **80** (1981) 215–19.
13. Hayashi, S., Fukaya, K. & Saito, H., Sintering of lanthanum chromite doped with zinc or copper. *J. Mater. Sci. Lett.*, **7** (1988) 457–8.
14. Anderson, H. U., Fabrication and property control of $LaCrO_3$ based oxides. *Processing of Crystalline Ceramics*, (Mater. Sci. Res., Vol. 11), ed. H. Palmour III, R. F. Davis & T. M. Hare. Plenum Press, New York, USA, 1978, pp. 469–77.
15. Bansal, K. P., Kumari, S., Das, B. K. & Jain, G. C., Electrical conduction in titania doped lanthanum chromite ceramics. *J. Mater. Sci.*, **16** (1981) 1994–8.
16. Koc, R. & Anderson, H. U. Liquid phase sintering of lanthanum chromite. *J. Eur. Ceramic Soc.*, **9** (1992) 285–92.
17. Nasrallah, M. M., Carter, J. D., Anderson, H. U. & Koc. R., Low temperature air sinterable $LaCrO_3$ and $YCrO_3$. In *Proc. 2nd International Symposium on SOFC's*, 1991, The Commission of the European Communities, Luxembourg, pp. 637–44.
18. Sakai, N., Kawada, T., Yokokawa, H., Dokiya, M. & Iwata, T., Sinterability and electrical conductivity of calcium-doped lanthanum chromites. *J. Mater. Sci.*, **25** (1990) 4531–4.
19. Sakai, N., Kawada., T., Yokokawa, H., Dokiya, M. &

Iwata, T., Thermal expansion of some chromium deficient lanthanum chromites. *Solid State Ionics*, **40/41** (1990) 394–7.
20. Sakai, N., Kawada, T., Yokokawa, H., Dokiya, M. & Iwata, T., Air sinterable (La,Ca)CrO_3 for SOFC interconnectors: some problems in powder preparation. The *Int. Fuel Cell Conf. Proc.*, Makulari, Japan, 3–6 Feb., 1992. NEDO, Tokyo, p. 365–8.
21. Sakai, N., Kawada, T., Yokokawa, H. & Dokiya, M., Chemical stability of (La,Ca)CrO_3 interconnects. *Proceedings of Zirconia V*, Melbourne, 16–21 Aug., 1992. Technomic Publishing Co., Lancaster, PA.
22. Pechini, M., Method of preparing lead and alkaline earth titanates and niobates and coating method using the same to form a capacitor. US Patent No. 3,330,697, July 1967.
23. Sakai, N., Kawada, T., Yokokawa, H., Dokiya, M. & Kojima, I. Liquid phase assisted sintering of calcium doped lanthanum chromites. *J. Am. Ceram. Soc.*, **76**(3) (1993) 609–16.
24. Milliken, C., Elangovan, S. & Khandkar, A., Mechanical and electrical stability of doped $LaCrO_3$ in SOFC applications. In *Proc. 3rd Int. Symp. on SOFC's*, ed. S. C. Singhal & H. Iwahara. The Electrochemical Society, Pennington, NJ, USA, 1993, pp. 335–43.
25. de Villiers, J. P. R., Mathias, J. & Muan, A., Phase relations in the system $CaO–Cr_2O_3–SiO_2$ in air and solid solutions relations along the $Ca_2SiO_4–Ca_3(CrO_4)_2$ join. *Trans. Inst. Mining Metallurgy Sect. C*, **96** (1987) C55–C62.
26. Pánek, Z. & Kanclír, E., A study of the reactions in the system Mg–Ca–Cr–O. Silikáty, **20**(2) (1976) 113–20.
27. Kashihara, T., Yoshioka, I., Kato, T., Arima, S. & Mohri, N. Studies on reducing reaction products of Cr–Ca system. *J. Metal Finishing Soc. Japan*, **26**(5) (1975) 9–13. (In Japanese).